Multibias TCAD Analysis of Trap Dynamics in GaN HEMTs

E. Catoggio(✉), S. Donati Guerrieri, and F. Bonani

Dipartimento di Elettronica e Telecomunicazioni, Politecnico di Torino, Turin, Italy
{eva.catoggio,simona.donati,fabrizio.bonani}@polito.it

Abstract. In this paper we exploit numerically efficient physical simulations to investigate the link between GaN HEMT low-frequency dispersion and the concentration of Fe induced buffer traps. We demonstrate that the sensitivity of the AC output conductance to trap concentration shows markedly different behavior according to the bias point, either in saturation or in the linear region at the HEMT knee voltage. The frequency dependency and the sensitivity of AC parameters in multiple bias points yield a deeper understanding of trap behavior and allow for easier identification of buffer trap signature in characterization data.

Keywords: GaN HEMTs · Nonlinear models · TCAD simulations

1 Introduction

TCAD (Technological CAD) can effectively link the fabrication process to semiconductor device performances in the very operating conditions within an integrated circuit. As such, TCAD represents one of the enabling modeling tools for Design Technology Co-Optimization (DTCO) [1–5]. Complementing experimental characterization, it provides advantages in terms of lower cost, faster generation of (synthetic) datasets, and a deep insight into the physical mechanisms underlying device operation, hence allowing for device optimization. In microwave integrated circuits (ICs), TCAD tools must include non conventional analyses (e.g., harmonic distortion, nonlinear behavior) and require, in particular for the emerging GaN ICs', advanced physical phenomena to be included in the simulation, namely the trap dynamic behavior, that can limit the device performance and reliability [6]. Typical effects of traps are the pronounced device long-term nonlinear memory, e.g., the gate and drain lag [7,8] and the Y parameters low-frequency dispersion [9–11]. On the other hand, it is often difficult to identify each trap (e.g., buffer, surface, interface) from the characterization of the overall device electrical behavior only.

Supported by the Italian MIUR under the PRIN 2017 Project "Empowering GaN-on-SiC and GaN-on-Si technologies for the next challenging millimeter-wave applications (GANAPP)".

C. Ciofi and E. Limiti (Eds.): SIE 2023, LNEE 1113, pp. 102–109, 2024.
https://doi.org/10.1007/978-3-031-48711-8_12

In this scenario, it is important to develop numerically efficient TCAD codes that can simulate the device sensitivity to trap parameters as well as position. An in-house software has been recently demonstrated [12,13] that explicitly implements the trap rate equations coupled to the drift-diffusion model. The model is solved in the frequency domain through the Harmonic Balance formalism, allowing for the investigation of both conversion effects and frequency dispersion due to traps. Such dispersion is especially important in the design of power amplifiers, since these effects are responsible for the frequency dependence of the output resistance and of the knee voltage [14]. To overcome the numerical burden of TCAD simulations, our implementation exploits a Green's Function approach for the fast calculation of device sensitivity starting from the "nominal" trap values. Furthermore, the technique concurrently makes available the *local sensitivity* for DC and AC parameters, thus allowing to identify the regions of the device where the trap parameter variations impact more the terminal electrical characteristics.

In this paper we demonstrate that the sensitivity of AC output admittance towards Fe-induced buffer trap concentration shows markedly different trends as a function of the DC operating conditions, whether it is chosen in the saturation region or at the knee voltage. In particular we show that the output admittance close to the knee voltage is especially sensitive to the trap density and both the real and imaginary parts can be used to identify the presence of buffer traps. The frequency behavior of the drain admittance Y_{DD} with varying trap concentration and bias can be used e.g., to complement measured data, to assess the presence of buffer traps and their density. It may also prove useful to provide the bias dependency of trap cut-off frequency in RC equivalent compact models.

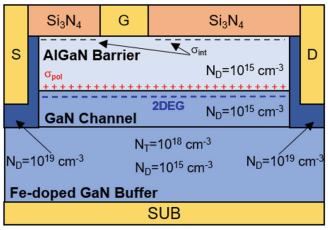

Thickness		Length	
Si_3N_4	100 nm	Gate	150 nm
AlGaN barrier	15 nm	Gate-Source	800 nm
GaN channel	5 nm	Gate-Drain	2000 nm
GaN buffer	2000 nm		

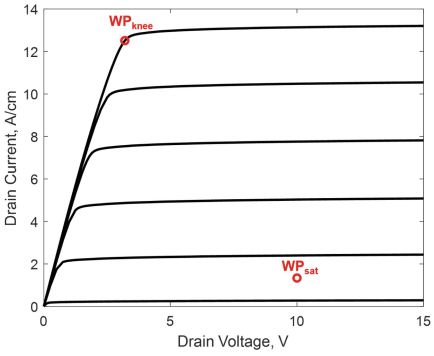

Fig. 1. Left: simulated HEMT structure. Right: static characteristics with nominal parameters varying the gate voltage from −2.5 V to 0 V with 0.5 V step. Markers denote the knee (WP_{knee}) and saturation (WP_{sat}) working points.

2 Device Structure

We simulate the 150 nm gate length HEMT shown in Fig. 1 (left), made of an AlGaN barrier with 25% Al mole fraction, and of a GaN layer with a residual donor doping of 10^{15} cm^{-3}. The channel region, 5 nm thick, is placed above a 2 μm deep buffer characterized by Fe-induced deep acceptor-like traps with concentration $N_T = 10^{18}$ cm^{-3}, nominal energy 0.45 eV below the conduction band edge, and electron and hole capture cross-sections $\sigma_n = \sigma_p = 3 \times 10^{-16}$ cm^{-3}. Fe-induced traps are simulated explicitly adding the trap rate equation and coupling it to the drift-diffusion physical model [12].

A fixed negative charge $\sigma_{\text{int}}/q = -2 \times 10^{12}$ cm^{-2} is added at the barrier/passivation interface. GaN spontaneous polarization and both AlGaN spontaneous and piezoelectric polarizations are included. The net polarization charge at the AlGaN/GaN interface is $\sigma_{\text{pol}}/q = 1.34 \times 10^{13}$ cm^{-2} with 90% activation. The in-house software implements the same polarization model as the Synopsys "Simplified strain model" [15]. Other details on the simulation settings are reported in [12].

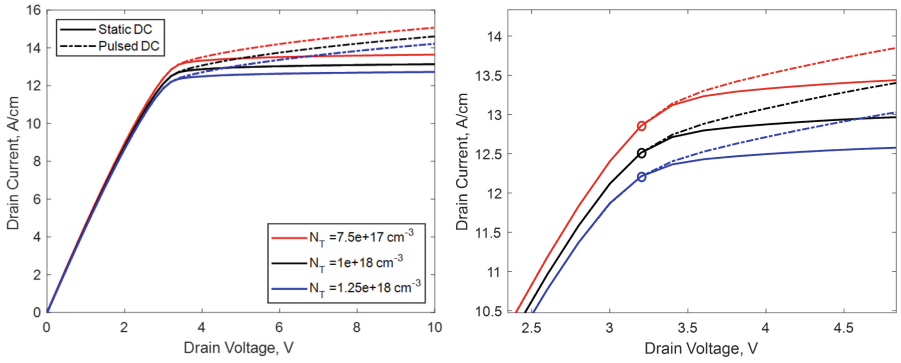

Fig. 2. Left: static (solid) and pulsed (dashed) output characteristics in the knee region and varying N_T. Right: zoom of the output characteristics in the knee region. The quiescent bias point used for pulsed simulations is set by $V_D = 3.2$ V and $V_G = 0$ V, shown by the circle marker.

3 Multibias Analysis of Trap Dynamics

First, the DC output characteristics are simulated for the nominal device, as shown in Fig. 1 (right). The device is characterized by the threshold voltage $V_{\text{th}} = -2.5$ V and $I_{D\text{ss}} = 13$ A/cm saturation current. We investigate how Fe-induced buffer traps impact the AC parameters in the two bias points reported in Fig. 1. The first working point selected in the knee region WP_{knee} is set to $V_D = 3.2$ V and $V_G = 0$ V, while the second one WP_{sat} is chosen in saturation

conditions at $V_D = 10$ V and $V_G = -2.22$ V. We now consider the effect of the variation of the buffer trap concentration in the range $\pm 25\% N_T$. Figure 2 (left) shows the static drain current at $V_G = 0$ V resulting from either static and pulsed DC TCAD analyses. We notice that with increasing N_T, the selected working point corresponding to $V_D = 3.2$ V gradually shifts from the linear to the saturation region, as shown in Fig. 2 (right): hence we expect that the output conductance exhibits a reduction with increasing N_T. Furthermore, the pulsed IV curves, also presented in Fig. 2, demonstrate that the trap dynamics affect only the saturation region, whereas the linear region is nearly insensitive to trap variations. Hence, a higher frequency dispersion can be expected in the output admittance in the saturation region, corresponding to the highest N_T value. On the other hand, the output characteristics at $V_G = -2.22$ V are reported in Fig. 3 for three N_T values, and they are compared to the corresponding pulsed DC analysis with quiescent bias of $V_D = 10$ V, i.e. the same $\mathrm{WP_{sat}}$ shown in Fig. 1 (right). The device operating condition is always in saturation for all the analyzed N_T values, despite it is evident that frequency dispersion induces a noticeable variation of the threshold voltage implying the varied shape of the characteristics [12]. The output conductance is nearly insensitive to N_T, but exhibits a very strong frequency dispersion, as shown by the different slopes between static and pulsed DC curves.

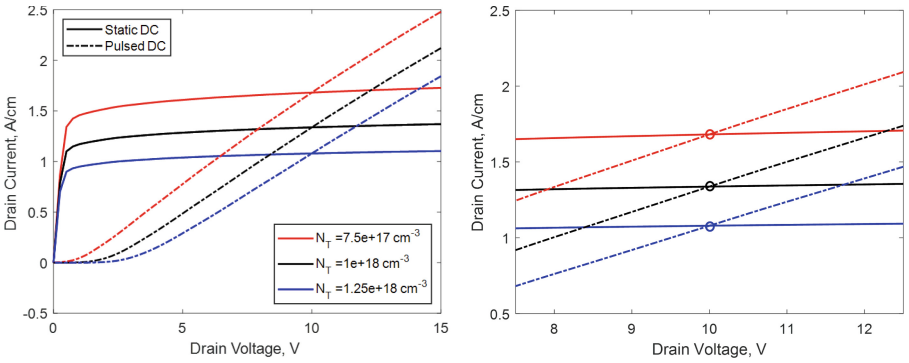

Fig. 3. Left: static (solid) and pulsed (dashed) output characteristics in saturation and varying N_T. Right: zoom of the output characteristics in the saturation region. The quiescent bias point used for pulsed simulations is set by $V_D = 10$ V and $V_G = -2.22$ V, shown by the circle marker.

In order to confirm such expectation, we carry out the AC analysis sweeping the frequency from DC to 1 MHz. At each frequency, the variation of the output admittance ΔY_{DD} is calculated varying the buffer trap concentration in the range $\pm 25\% N_T$ using the fast GF analysis. Figure 4 shows the real part of the simulated Y_{DD} parameter as a function of frequency and buffer trap concentration, both in the knee bias point (left) and at saturation (right). As expected,

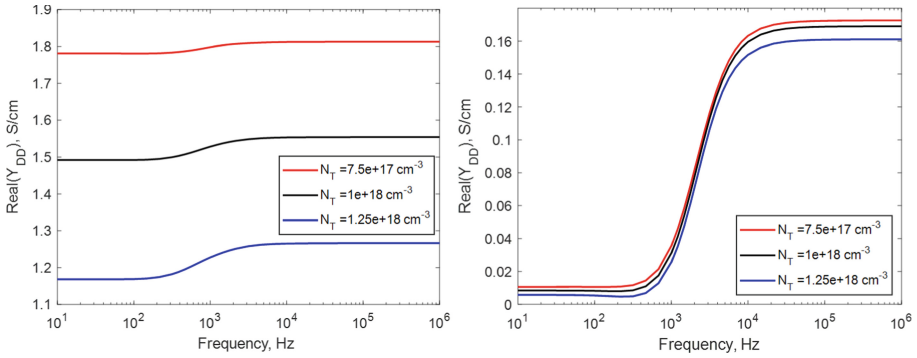

Fig. 4. Real part of Y_{DD} as a function of frequency and trap concentration. Left: knee region. Right: saturation region.

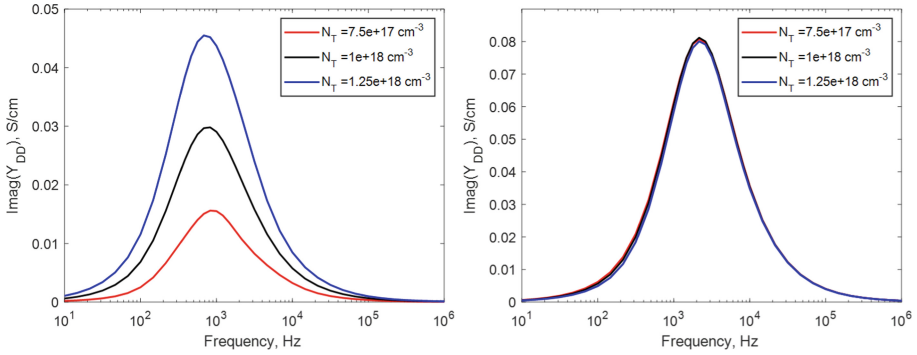

Fig. 5. Imaginary part of Y_{DD} as a function of frequency and trap concentration. Left: knee region. Right: saturation region.

Real(Y_{DD}) is directly connected to the slope of the static output characteristics at low frequency and of the pulsed curves at high frequency, see Fig. 2 for the knee and Fig. 3 for the saturation case, respectively. It is clear that the knee condition makes the trap signature more evident in terms of the output conductance variation. Moreover, the frequency dispersion behavior slightly affects Real(Y_{DD}) in the knee region, but represents a signature of traps in saturation despite the N_T dependence is not clearly detected.

Trap signature becomes even more evident inspecting the imaginary part of the output admittance, reported in Fig. 5 as a function of both frequency and buffer trap concentration. The frequency behavior clearly shows a peak related to the trap dynamics at 750 Hz in the knee region and at 2.15 kHz in the saturation region. This frequency trend is well known to be a signature of traps dynamics, as reported, e.g., in [11]. Notice, though, that while the knee bias peak frequency shifts very mildly towards lower values with increasing trap concentration, the

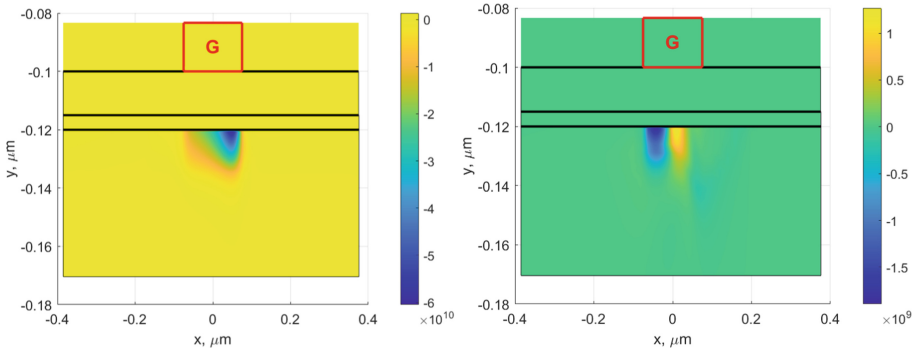

Fig. 6. Local source for the real part of Y_{DD} corresponding to +25% N_T variation at the peak frequency of Fig. 4. Left: knee region. Right: saturation region.

peak height shows instead a significant sensitivity to N_T. On the contrary, the imaginary part is nearly insensitive to N_T in saturation.

Overall, the combined analysis of real and imaginary parts shows that the knee bias condition is more apt at identifying the trap concentration.

Our approach based on GFs allows for an even deeper insight of the trap impact on AC parameters through the local variation sources. In fact, the local variation source of Y_{DD} yields, once integrated over the device cross section, the variation of the Y_{DD} parameter with respect to the nominal value [12]. Figure 6 shows the distributed source for the real part of Y_{DD} at peak frequency for a variation of $+25\%N_T$. At the knee bias, the local source is distributed under the whole gate contact and assumes negative values, leading to a reduction of Real(Y_{DD}). Moreover, it shows a strongly negative peak towards the drain contact. A different behavior can be noticed in saturation region, where the local source shows a negative peak towards the source and a positive peak in the mid-channel region. The saturated portion of the channel towards the drain does not affect the variation of Real(Y_{DD}). The local variation source of the imaginary part of Y_{DD} is reported in Fig. 7 at peak frequency for a variation of $+25\%N_T$. The local source is different for the two bias points, and markedly shifted towards the drain at the knee voltage, while more at the source in saturation. Furthermore, a compensation of negative and positive peaks results in a nearly null variation of Y_{DD} in saturation. On the contrary, the local source is always positive at the knee bias, giving a positive variation of Imag(Y_{DD}).

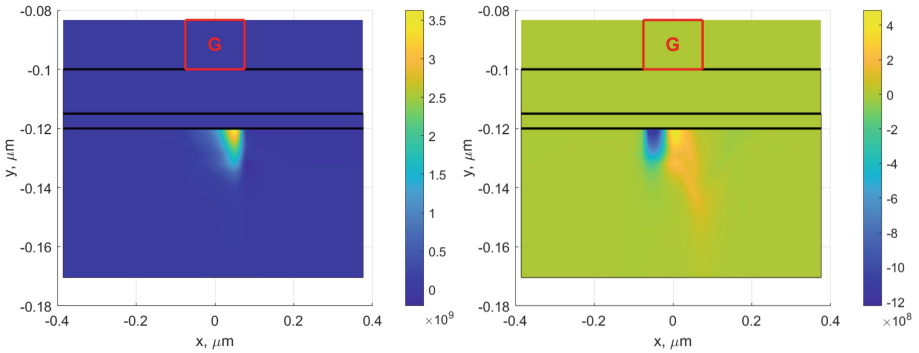

Fig. 7. Local source for the imaginary part of Y_{DD} corresponding to +25% N_T variation at the peak frequency of Fig. 5. Left: knee region. Right: saturation region.

4 Conclusions

We have exploited an in-house simulator implementing the drift-diffusion model coupled to the trap rate equations to investigate the sensitivity of the AC output admittance to the Fe-induced buffer trap concentration variations in an AlGaN/GaN HEMT device at different bias points. We have demonstrated that the concurrent analysis of real and imaginary parts of Y_{DD} at the knee voltage can be used to identify both the trap concentration and the frequency dispersion. The effect of traps on the AC parameters is investigated also at the microscopic level using the local variation sources. Despite in this work we have analyzed only frequency dispersion due to traps, the implemented code can address other dispersion effects, e.g., thermal [16], concurrently with traps dynamics. This makes it possible to develop compact models, e.g. extending X-parameters [17], to be used in a technology aware microwave stage design.

References

1. Wen, Z., Mao, S., Wu, Y., Xu, R., Yan, B., Xu, Y.: A quasi-physical large-signal statistical model for 0.15 μm AlGaN/GaN HEMTs process. In: 2019 IEEE MTT-S International Microwave Symposium (IMS) (2019). https://doi.org/10.1109/MWSYM.2019.8700840
2. Williams, S., Varahramyan, K.: A new TCAD-based statistical methodology for the optimization and sensitivity analysis of semiconductor technologies. IEEE Trans. Semicond. Manuf. **13**, 208–218 (2000). https://doi.org/10.1109/66.843636
3. Chordia, A., Hemaram, S., Tripathi, J.N.: A swarm intelligence based automated framework for variability analysis. In: 2020 IEEE MTT-S Latin America Microwave Conference (2020). https://doi.org/10.1109/LAMC50424.2021.9602347
4. Donati Guerrieri, S., Ramella, C., Catoggio, E., Bonani, F.: Bridging the gap between physical and circuit analysis for variability-aware microwave design: modeling approaches. Electronics **11**(6), 860 (2022). https://doi.org/10.3390/electronics11060860

5. Donati Guerrieri, S., Ramella, C., Catoggio, E., Bonani, F.: Bridging the gap between physical and circuit analysis for variability-aware microwave design: power amplifier design. Electronics **11**(18), 2832 (2022). https://doi.org/10.3390/electronics11182832
6. Meneghesso, G., Verzellesi, G., Danesin, F., Rampazzo, F., Zanon, F., Tazzoli, A., Meneghini, M., Zanoni, E.: Reliability of GaN high-electron-mobility transistors: state of the art and perspectives. IEEE Trans. Device Mater. Reliab. **8**(2), 332–343 (2008). https://doi.org/10.1109/TDMR.2008.923743
7. Zagni, N., Verzellesi, G., Chini, A.: Temperature-independent current dispersion in 0.15 μm AlGaN/GaN HEMTs for 5G applications. Micromachines **13**(12), 2244 (2022). https://doi.org/10.3390/mi13122244
8. Angelotti, A.M., Gibiino, G.P., Santarelli, A., Florian, C.: Experimental characterization of charge trapping dynamics in 100-nm AlN/GaN/AlGaN-on-Si HEMTs by wideband transient measurements. IEEE Trans. Electron Devices **67**(8), 3069–3074 (2020). https://doi.org/10.1109/TED.2020.3000983OI
9. Beleniotis, P., Schnieder, F., Chevtchenko, S., Rudolph, M.: Localization of trapping effects in GaN HEMTs with pulsed S-parameters and compact models. In: 2022 17th European Microwave Integrated Circuits Conference (EuMIC) (2022). https://doi.org/10.23919/Eu-MIC54520.2022.9923511
10. Raffo, A., Vadalà, V., Bosi, G., Giofrè, R., Vannini, G.: 150-nm GaN HEMT degradation under realistic load-line operation. In: 2022 17th European Microwave Integrated Circuits Conference (EuMIC) (2022). https://doi.org/10.23919/EuMIC54520.2022.9923438
11. Raja, P.V., Subramani, N.K., Gaillard, F., Bouslama, M., Sommet, R., Nallatamby, J.C.: Identification of buffer and surface traps in Fe-doped AlGaN/GaN HEMTs using Y21 frequency dispersion properties. Electronics **10**(24), 3096 (2021). https://doi.org/10.23919/EuMIC54520.2022.9923438
12. Catoggio, E., Donati Guerrieri, S., Bonani, F.: TCAD modeling of GaN HEMT output admittance dispersion through trap rate equation Green's functions. Electronics **12**(11), 2457 (2023). https://doi.org/10.3390/electronics12112457
13. Donati Guerrieri, S., Ramella, C., Bonani, F., Ghione, G.: Efficient sensitivity and variability analysis of nonlinear microwave stages through concurrent TCAD and EM modeling. IEEE J. Multiscale Multiphys. Comput. Tech. (2019). https://doi.org/10.1109/jmmct.2019.2962083
14. Subramani, N.K.: Physics-based TCAD device simulations and measurements of GaN HEMT technology for RF power amplifier applications, Ph.D. Dissertation, University of Limoges, Limoges (2017). https://tel.archives-ouvertes.fr/tel-01702325
15. Synopsys Sentaurus. https://www.synopsys.com/silicon/tcad/device-simulation/sentaurus-device.html
16. Catoggio, E., Donati Guerrieri, S., Bonani, F.: Efficient TCAD thermal analysis of semiconductor devices. IEEE Trans. Electron Devices **68**(11), 5462–5468 (2021). https://doi.org/10.1109/TED.2021.3076753
17. Donati Guerrieri, S., Bonani, F., Ghione, G.: Linking X parameters to physical simulations for design-oriented large-signal device variability modeling. In: 2019 IEEE MTT-S International Microwave Symposium (IMS) (2019). https://doi.org/10.1109/mwsym.2019.8700869